JOURNAL OF PHYSICAL ORGANIC CHEMISTRY
J. Phys. Org. Chem. 2004; **17:** 890–897
Published online in Wiley InterScience (www.interscience.wiley.com). DOI: 10.1002/poc.783

meso-Tetratolylporphyrins substituted by pyridinium groups: aggregation, photophysical properties and complexation with DNA

K. Procházková,[1] Z. Zelinger,[1] K. Lang[2] and P. Kubát[1]*

[1]J. Heyrovský Institute of Physical Chemistry, Academy of Sciences of the Czech Republic, Dolejškova 3, 182 23 Prague 8, Czech Republic
[2]Institute of Inorganic Chemistry, Academy of Sciences of the Czech Republic, 250 68 Rıež, Czech Republic

Received 19 November 2003; revised 29 January 2004; accepted 17 February 2004

ABSTRACT: The aggregation behavior, binding to DNA and photophysical properties of *meso*-tetratolylporphyrins substituted with two (**P_2**), three (**P_3**) and four (**P_4**) pyridinium groups were studied using UV–visible and transient spectroscopy, resonance light scattering, circular dichroism and time-resolved luminescence of singlet oxygen. In aqueous solutions porphyrins **P_2**–**P_4** were present as monomers and aggregates of H- and J-type. The concentration ratio of monomer to aggregates was controlled by the number of cationic substituents, by ionic strength and by temperature. Porphyrin **P_4** was predominantly monomeric and was externally bound to calf thymus DNA with a binding constant of 1.2×10^6 M^{-1}. Porphyrins **P_3** and **P_2** self-assembled on the DNA backbone to form chiral assemblies not affecting the duplex melting point. The lifetimes of the triplet states of monomeric **P_3** and **P_4** increased after binding to DNA; however, this did not prevent the formation of singlet oxygen, $^1O_2$. Copyright © 2004 John Wiley & Sons, Ltd.

KEYWORDS: porphyrin; aggregates; DNA; photophysics

INTRODUCTION

Cationic porphyrins have attracted considerable attention owing to their binding affinity to nucleic acids[1] and their ability to cleave DNA selectively,[2] to inhibit human telomerases[3] and serve as vehicles for oligonucleotide delivery to tumors.[4] The photoinduced action of porphyrins is usually connected with the production of singlet oxygen,[5] a very reactive species that is able to oxidize G-rich sequences of nucleic acids.[6] Porphyrin derivatives, depending on their structure and coordinated metal, including axial ligands, display different preferences not only for particular binding modes, but also for different DNA sequences. In general, three binding models have been described for the interaction of cationic porphyrins with DNA:[7] (i) intercalation, (ii) outside groove binding and (iii) outside binding with self-stacking. The last mode leads to the formation of organized helical porphyrin structures on the DNA template.[8–10] The rational functionalization of the porphyrin periphery renders derivatives of a different charge, size and hydrophobicity. The interest in porphyrins bearing polar–lipophilic substituents or substituents with low polarizability stems from the fact that such substituents can facilitate the transport of the porphyrin molecule through biological membranes.[11,12] However, lipophilic substituents cause the porphyrins to aggregate in aqueous solutions. Before any potential application of such porphyrins could be considered, the aggregation behavior must be addressed.

Aggregation of porphyrins in aqueous solution both with and without the presence of multipoint templates such as nucleic acids has an enormous impact on the ability of porphyrins to generate singlet oxygen and to cleave nucleic acids. The coupling of transition dipole moments of strongly absorbing porphyrin derivatives results in dramatic perturbations to the electronic spectra of aggregates.[13] The nomenclature distinguishes H-aggregates with blue-shifted and J-aggregates with red-shifted Soret bands in which the monomer transition dipoles are perpendicular and parallel to the line connecting neighboring molecule centers, respectively. Strongly coupled J-aggregates with delocalized excitonic states are especially interesting because they may possess optical properties such as superradiance.[14] Most attention has been focused on the aggregation of anionic 5,10,15,20-tetrakis(4-sulfonatophenyl)porphyrin forming J-aggregates in aqueous solution at low pHs and high ionic strength.[15] On the other hand, tetracationic 5,10,15,20-tetrakis(*N*-methylpyridinium-4-yl)porphyrin (TMPyP) exists as a monomer in water even at low pH and in the presence of concentrated inorganic salts.[16] It

**Correspondence to:* P. Kubát, J. Heyrovský Institute of Physical Chemistry, Academy of Sciences of the Czech Republic, Dolejškova 3, 182 23 Prague 8, Czech Republic.
E-mail: kubat@jh-inst.cas.cz.
Contract/grant sponsor: Grant agency of the Czech Republic; *Contract/grant numbers:* 203/01/0634; 203/02/0420; 203/04/0426.

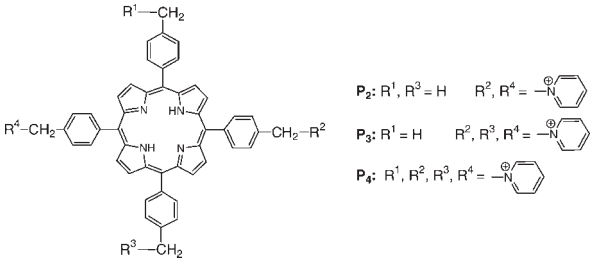

Figure 1. Molecular structures of porphyrins $\mathbf{P_2}$, $\mathbf{P_3}$ and $\mathbf{P_4}$

has been proposed that the positive charges at the periphery of TMPyP delocalized over the porphyrin ring result in electrostatic repulsive forces, thereby preventing aggregate formation.[17] By way of contrast, other cationic porphyrins aggregate spontaneously in neutral aqueous solutions forming various types of aggregates.[18,19]

The properties of tetracationic porphyrins have been studied in detail,[17,18,20–22] whereas little consideration has been devoted to porphyrins bearing two or three cationic substituents.[23] In this paper, we report the properties of peripherally substituted tetratolylporphyrins $\mathbf{P_2}$–$\mathbf{P_4}$ with two, three or four pyridinium groups (Fig. 1), including aggregation of porphyrins, photophysical properties and complexation with DNA. The pyridinium moieties of these cationic porphyrins are separated from the porphyrin ring by methylene spacers, preventing the delocalization of the positive charge within the porphyrin π-electron system by direct coupling. The positive charges of these cationic porphyrins can impact the charge distribution of the porphyrin ring through inductive effects only. Therefore, monomeric $\mathbf{P_2}$–$\mathbf{P_4}$ can be expected to display similar photophysical properties, but with considerable differences in self-aggregation and complexation towards DNA. Here we show that the number of charged peripheral substituents effectively controls hydrophobic/electrostatic forces and the nature of porphyrin aggregates and porphyrin–DNA forms.

EXPERIMENTAL

Materials

The syntheses of 5,15-bis(α-[pyridinium]-4-tolyl)-10,20-bis(4-tolyl)porphyrin ($\mathbf{P_2}$), 5,10,15-tris(α-[pyridinium]-4-tolyl)-20-(4-tolyl)porphyrin ($\mathbf{P_3}$) and 5,10,15,20-tetrakis(α-[pyridinium]-4-tolyl)porphyrin ($\mathbf{P_4}$) bromide salts (Fig. 1) have been described previously.[19,21] Stock solutions were prepared in methanol (300–500 μM) where porphyrins are in monomeric form. 5,10,15,20-Tetrakis(4-sulfonatophenyl)porphyrin tetrasodium salt (TPPS), (Aldrich), 5,10,15,20-tetrakis(*N*-methylpyridinium-4-yl)porphyrin tetra-4-tosylate salt (TMPyP), (Aldrich), calf thymus double-stranded DNA (Sigma) and D_2O (98%) were used as received. The concentration of DNA, calculated in base pairs, was determined from UV spectra using ε_{260} of $1.31 \times 10^4\ \text{M}^{-1}\,\text{cm}^{-1}$.[24] Experiments were performed in air-saturated 20 mM phosphate buffer (pH 7.0) at temperatures in the range 20–90 °C; the ionic strength was adjusted by the addition of NaCl.

Spectral measurements

All UV–visible absorption spectra were recorded using a Perkin-Elmer Lambda 19 spectrophotometer. The aggregation and binding were evaluated using spectral changes in the corresponding Soret bands at different DNA (in base pairs) to porphyrin molar concentration ratios *R*. Absorbance titrations were conducted by adding a concentrated stock solution of DNA directly to a porphyrin solution (1.0–5.0 μM) in a 10 mm cuvette. All measurements were corrected for dilution caused by the volume of added solution. Binding experiments were performed in solutions containing 20 mM phosphate buffer (pH 7.0) and 100 mM NaCl at 25 or 37 °C. Melting curves were recorded at 258 nm in 20 mM phosphate buffer (pH 7.0) with 50 mM NaCl using the heating rate of $0.5\ ^\circ\text{C}\,\text{min}^{-1}$. The conditions used for thermal experiments were a compromise to obtain suitable aggregation/deaggregation behavior of porphyrins at higher temperatures, binding of porphyrin aggregates at the DNA surface, monomerization/self-association of porphyrins on the DNA exterior and to minimize stabilization of the DNA duplex by ionic strength. Resonance light-scattering (RLS) experiments were performed on a Perkin-Elmer LS 50B luminescence spectrophotometer using simultaneous scans of excitation and emission monochromators through a range 300–600 nm. Induced circular dichroism (CD) spectra were measured on a Jobin Yvon-Spex CD 6 instrument.

Laser flash photolysis experiments were performed with a Lambda Physik FL 3002 dye laser (414–424 nm, output 0.05–5 mJ per pulse, pulse width ~28 ns). The transient spectra were measured within 300–600 nm on a laser kinetic spectrometer (Applied Photophysics, UK). The time profiles of the triplet state decay were recorded at 460 nm using a 250 W Xe lamp equipped with a pulse unit and an R928 photomultiplier (Hamamatsu). The samples were saturated by air or by oxygen, where appropriate, and oxygen was removed from the solution by argon purging. In argon-saturated solutions decay curves were averaged using 10–500 single traces to decrease the noise level. Measurements were performed with different porphyrin concentrations (4.0–5.6 μM) and the standard deviation presented in Table 1 was obtained by statistical treatment of independent experiments. Time-resolved near-infrared luminescence of singlet oxygen O_2 ($^1\Delta_g$) at 1270 nm was monitored with a Ge diode (Judson J16–8SP, USA) in conjunction with a 1270 nm interference filter. The quantum yields of singlet oxygen, Φ_Δ, were estimated by the comparative method using TPPS as a standard [$\Phi_\Delta = 0.63$ (ref. 25)] at an excitation

energy of 350 μJ. In this energy region, the intensity of a luminescence signal is proportional to the incident energy. Optically matched solutions at an excitation wavelength of 308 nm ($A_{308} = 0.100 \pm 0.002$) were prepared in an aqueous solution containing 50% D_2O to increase the singlet oxygen lifetime.

RESULTS AND DISCUSSION

Aggregation in aqueous solution

A detailed description of the behavior of porphyrins in aqueous solutions is a prerequisite for understanding the nature of the interaction of porphyrins with nucleic acids. Porphyrins **P_2**–**P_4** (Fig. 1) were monomeric in methanol and showed typical porphyrin UV–visible spectra with the Soret band at 414 nm and molar absorption coefficients ε_{414} of $(3.9 \pm 0.1) \times 10^5$, $(4.2 \pm 0.1) \times 10^5$ and $(4.0 \pm 0.2) \times 10^5\ \text{M}^{-1}\,\text{cm}^{-1}$ for **P_2**, **P_3** and **P_4**, respectively.

Porphyrin **P_4**, the most hydrophilic compound, was monomeric in buffer with 0.1 M NaCl, as indicated by the validity of the Lambert–Beer law and the narrow Soret band at 414 nm [Fig. 2(a)]. As the hydrophobicity of the molecule increases in the series **P_4** < **P_3** < **P_2**, the spectral behavior of **P_2** and **P_3** in aqueous solutions was more complex. Porphyrins **P_2** and **P_3** were soluble in water, but a splitting of the Soret band, some hypochromicity and deviations from the Lambert–Beer law pointed to extensive aggregation [Fig. 2(b), (c)]. The degree of aggregation was strongly increased at higher ionic strength (controlled by adding NaCl) and decreased at higher temperature. The UV–visible spectra of **P_3** show that at high ionic strength an intensive band at 438 nm appeared compared with a solution of low ionic strength [cf. Figs. 2(b) and 3(a)]. Complete deaggregation was observed at higher temperatures as demonstrated by Fig. 4(a), where the absorption band at 438 nm disappeared at 70 °C. Considering the positive charge located at the porphyrin periphery and the facilitation of aggregation by increasing ionic strength, electrostatic interactions are evidently a significant factor in stabilizing porphyrin aggregates due to neutralization of the high positive charge density of the aggregate. In addition, the hydrophobic forces[26] could also be important, especially in the case of dicationic **P_2**.

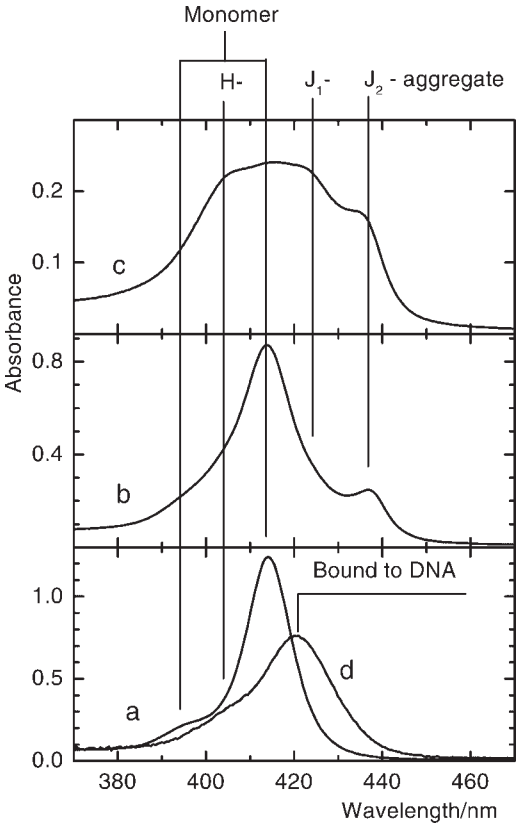

Figure 2. UV–visible spectra: Soret region of monomeric **P_4** (a), partially monomeric **P_3** (b), highly aggregated **P_2** (c) and of **P_4** monomer bound to DNA, $R = 78$ (d) in 20 mM phosphate buffer (pH 7.0), 0.1 M NaCl, 22 °C, porphyrin concentration 3.2 μM

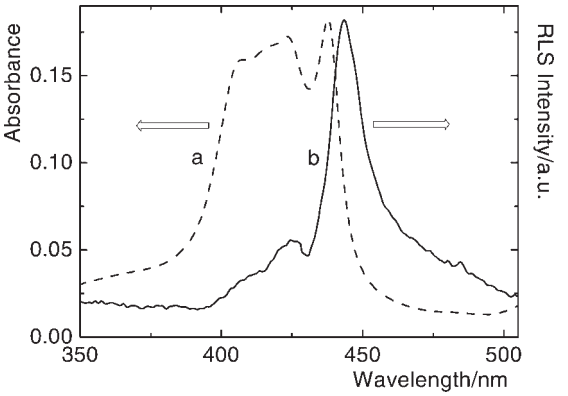

Figure 3. UV–visible absorption (a) (dashed line) and RLS (b) (solid line) spectra of **P_3** (2.0 μM) in 20 mM phosphate buffer (pH 7.0), 0.8 M NaCl, 22 °C

The Kasha theory, i.e. the exciton coupling model in its simple exciton point-dipole form, can be useful for the prediction of a structure of porphyrin aggregates.[13,27,28] A blue-shifted Soret band is indicative of a face-to-face arrangement of the porphyrin units assigned as H-aggregate while a parallel arrangement of the porphyrin units leads to a red shift of the Soret band. These aggregates are termed J-aggregates. The energy levels of both types of aggregates are schematically presented in Fig. 5.

In order to specify the respective aggregate forms, the Soret bands were analyzed as demonstrated in detail in Fig. 4 and made practical in Figs 2 and 4. The Soret bands can be characterized by a Voigtian profile in the temperature region from −250 to 25 °C.[29] The Voigtian profile is a convolution of a natural Lorentzian bandwidth with a Gaussian part containing a temperature-dependent component that is more significant at higher temperatures. Hence the Soret bands of **P_2**–**P_4** at temperatures between

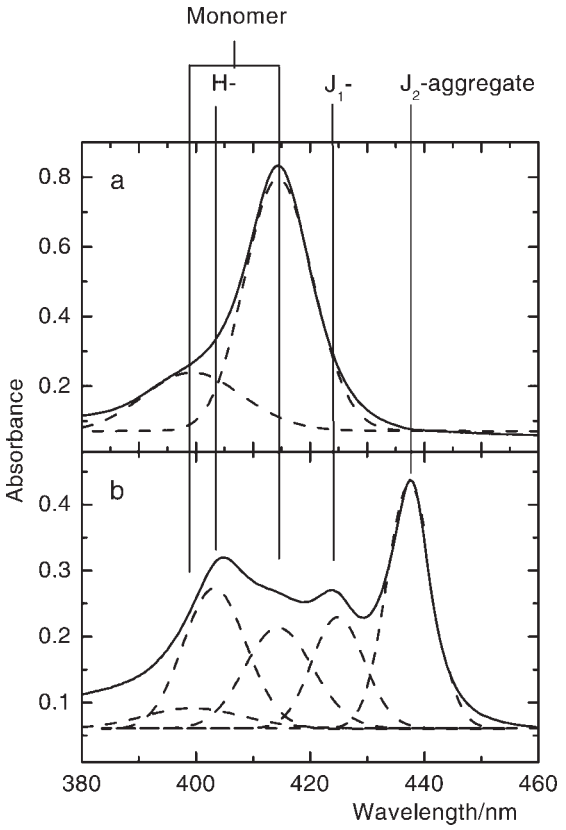

Figure 4. Soret region of monomeric $\mathbf{P_3}$ (3.0 μM) recorded at 70 °C (a) and of aggregates formed after cooling to 22 °C (b). The individual sub-bands were fitted by a combination of Gaussian functions in wavenumber units ($1/\lambda$). Experiments were carried out in 20 mM phosphate buffer (pH 7.0), 0.5 M NaCl

20 and 80 °C were analyzed by a combination of Gaussian functions. The Soret band of the monomer [Figs 2(a) and 4(a)] consists of two bands centered at 399 and 414 nm; a weak shoulder at 399 nm is of vibronic origin.[30] Evidently the position is not affected by the number of peripheral substituents. The envelopes of the spectra were generally analyzed with up to five Gaussians in order to obtain satisfactory fits [Fig. 4(b)]. These fits were composed of two bands of the monomer (399, 414 nm), a blue-shifted band of H-aggregate (403 nm) and two bands at 424 and 438 nm attributed to two major populations of J-aggregates. In general, J-aggregates are characterized by sharp absorption bands relative to the monomer band, a result of exciton delocalization over a number of monomer units.[31] In accordance with this, both bands at 424 nm (J_1) and 438 nm (J_2) are sharper than the monomer band at 414 nm [Fig. 4(b)]. The sharp band at 438 nm in particular indicates a narrow distribution of the local stacking structural arrangement within the J_2-aggregate. The positions of the respective Soret bands are the same for $\mathbf{P_2}$–$\mathbf{P_4}$ (Figs 2 and 4), indicating that the number of cationic substituents does not influence the energy levels of the porphyrin moiety. The observed energy transitions are depicted schematically in Fig. 5.

The aggregation number can be qualitatively estimated using RLS experiments and usually exceeding thousands of porphyrin units.[32] The method is convenient because the amount of scattered light is directly proportional to the volume of particles and monomeric molecules and small oligomers show no enhanced scattering.[9,32] The RLS peak at 445 nm [Fig. 3(b)] indicated an enhancement of the scattered light intensity due to the presence of extended J-aggregates [Fig. 3(a)]. It also revealed that H-aggregate and J_1-aggregate consist of a significantly lower number of porphyrin units (Fig. 5).

Photophysical properties

The photophysical properties of $\mathbf{P_2}$–$\mathbf{P_4}$ are summarized in Table 1. Transient triplet–triplet spectra had broad absorption maxima at 450–460 nm, which are typical for porphyrins.[21] The lifetime of the triplet states was

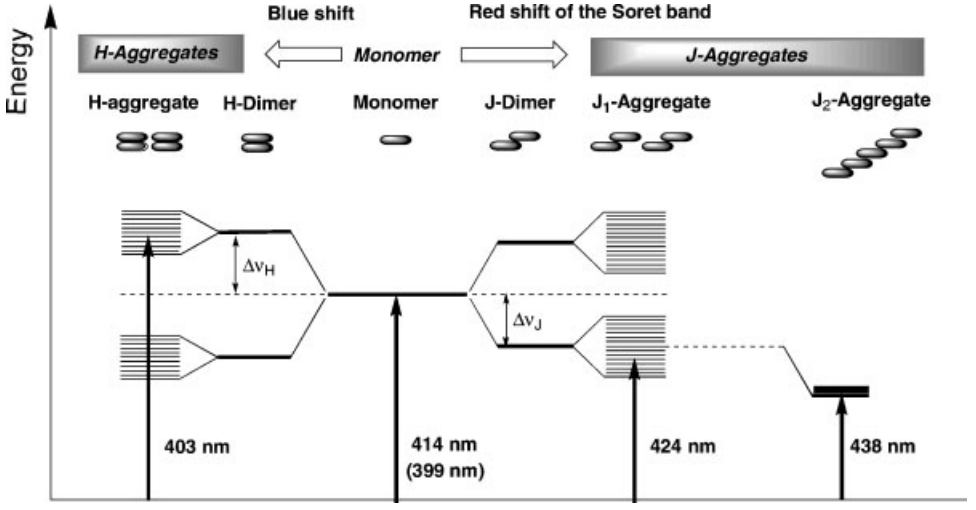

Figure 5. Energy level scheme of splitting of the Soret bands due to dimer and aggregate formation; only allowed transitions are shown

Table 1. Triplet states of **P_4**–**P_2** (4.0–5.6 μM) in solution and after binding to DNA ($R = 110$): the lifetimes in air-saturated and oxygen-free buffer τ_T (20 mM phosphate buffer, pH 7.0, 0.1 M NaCl) and the quantum yields of singlet oxygen Φ_Δ [D_2O—H_2O (1:1)]

	τ_T (μs)		
Compound	Air	Argon	Φ_Δ
P_4	2.0 ± 0.1	591 ± 40	0.59
P_3	2.6 ± 0.2	467 ± 37	0.42
P_2	2.1 ± 0.9	434 ± 90	<0.01[a]
P_4–DNA	12.2 ± 0.2[b]	—	—
P_3–DNA	17.1 ± 0.3[b]	—	—

[a] No signal owing to extensive porphyrin aggregation.
[b] Biexponential quenching kinetics; the faster process corresponds to free porphyrin, which is in the equilibrium with the bound molecules (slower process).

>400 μs. The triplet states were quenched by molecular oxygen with a bimolecular rate constant, k_q, of the order of $10^9\ M^{-1}\ s^{-1}$, yielding $^1O_2$. Hence the lifetime of the triplet states in air-saturated aqueous solutions was about 2 μs.

Since photosensitized reactions are mostly mediated by $^1O_2$, the quantum yield of singlet oxygen formation, Φ_Δ, produced by sensitizers is an important photophysical quantity. The Φ_Δ values were found to be 0.42 and 0.59 for **P_3** and **P_4** in water, respectively. These values are closely comparable to those of porphyrin sensitizers.[33] In contradiction, **P_2** did not produce singlet oxygen ($\Phi_\Delta <$ 0.01). This can be explained by extensive aggregation of **P_2** (see earlier). Exciton coupling between stacked porphyrin units causes fast relaxation of the excited states. This highly competitive process reduces considerably the formation of the triplet states and consequently of $^1O_2$ as reported for aggregated porphyrins.[34] We also attribute the lower Φ_Δ of **P_3** to a contribution of aggregates, although a low concentration of **P_3** ($\sim$0.4 μM) in pure water was used to minimize aggregation effects.

Binding to DNA and consequences to photophysics

Porphyrins were titrated with aliquots of a DNA solution and the corresponding spectral features in UV–visible spectra were recorded as a function of R (molar concentration ratio of DNA in base pairs to porphyrin). The Q bands in the visible region underwent minor changes; however, the Soret bands exhibited changes that permitted monitoring of the interaction of porphyrins with DNA.

The Soret band of **P_4** underwent a red shift from 414 to 421 nm with 40% hypochromicity after adding a stock solution of DNA [cf. Fig. 2(a) and (d)]. Since **P_4** is monomeric, the observed spectral perturbations are due to the association of **P_4** with DNA. The recorded data were cast into the McGhee–von Hippel binding model

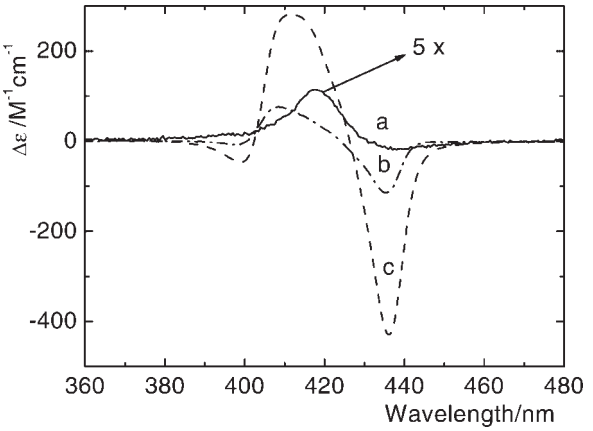

Figure 6. Induced CD spectra of **P_4** (a) ($R = 25$, 0.1 M NaCl, signal multiplied five times), **P_3** (b) ($R = 126$, buffer) and **P_3** (c) ($R = 126$, 0.33 M NaCl) in the presence of DNA. Experiments were performed in 20 mM phosphate buffer (pH 7.1), 22 °C

and the resultant binding constant of $(1.2 \pm 0.2) \times 10^6\ M^{-1}$ (Ref. 21) was closely comparable to those reported for other cationic porphyrins.[10] The exclusion parameter obtained of 8.1, which describes the number of base pairs removed by the binding, and a small red shift of the Soret band indicate that **P_4** is bound externally to the DNA surface.[21] The induced CD spectra can further corroborate the binding mode. The sign of the induced CD depends on the relative orientation of the transition dipole moment of a binder relative to that of the DNA bases.[35] As a rule, intercalative binding of the porphyrin chromophore with degenerate in-plane polarization of π–π transitions induces a negative CD signal in the Soret region, whereas external (groove) binding induces a positive signal.[7,10,36,37] The observed induced single positive band [Fig. 6(a)] indicates that **P_4** has a strong interaction with the bases of DNA and it is accordance with groove-bound porphyrin. Then, the planes of bound **P_4** are oriented at angles of roughly 45° with respect to the axis of DNA.[36] The specific binding configuration depends on the porphyrin loading since the position of the band is affected by R.[21] Intercalation of **P_4** between base pairs of the DNA matrix is evidently excluded owing to steric obstacles imposed by the bulky peripheral substituents.

Monomeric **P_3** bearing three pyridinium substituents showed the absorption band at 421 nm after binding to DNA (cf. spectra in Fig. 7, dashed lines). The large hypochromicity suggests considerable perturbation of the porphyrin π system due to the association with DNA. At high excess of DNA ($R > 40$) the amount of H- and J-aggregates was reduced, as indicated by a strong decrease in the absorbances at 403 and 438 nm concomitant with an increase in the absorbance of bound monomeric **P_3** at 421 nm [Fig. 7(b)]. The rate of this deaggregation process was controlled by the DNA concentration (i.e. by amount of negatively charged binding

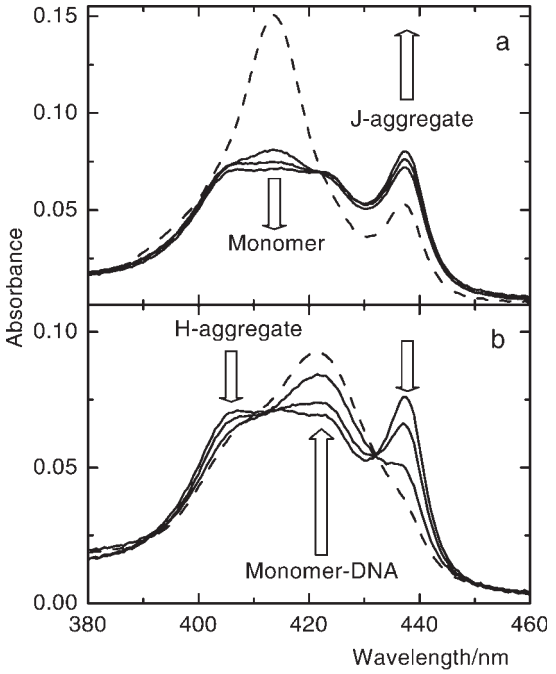

Figure 7. Changes in the Soret region of 1.0 μM **P_3** with increasing concentration of DNA: (a) formation of J-aggregates, $R = 0$ (dashed line), 2, 7 and 13; (b) binding to DNA at $R = 13$, 43 and 182 ($R = 182$, 120 min standing: dashed line). Arrows designate spectral changes due to increasing concentration of DNA. Experiments were carried out in 20 mM phosphate buffer (pH 7.0), 0.1 M NaCl, 22 °C

sites) and by ionic strength, since a high concentration of ions can shield the positive charge of aggregates and stabilize them. The binding-induced changes in the UV–visible spectra [Fig. 7(b)] were accompanied by intensive RLS profiles, confirming the formation of extended porphyrin assemblies on the DNA surface. The interaction of **P_3** with DNA also induced a bisignate CD spectrum with $\Delta\varepsilon$ near the maximum of the absorption band of bound **P_3** [Fig. 6(b)]. The positive band appeared at 409 nm ($\Delta\varepsilon = 77\ M^{-1}\ cm^{-1}$) and the negative band at 435 nm ($\Delta\varepsilon = -114\ M^{-1}\ cm^{-1}$). The porphyrin moiety is planar and symmetrical and does not possess natural optical activity, hence the induced chirality is due only to binding of **P_3** to DNA, a right-handed template. Such strong exciton coupling in the porphyrin Soret region is generally taken as evidence of groove binding or external stacking.[35] The intensity of the bisignate signal increased considerably at high ionic strength with a positive band at 412 nm ($\Delta\varepsilon = 281\ M^{-1}\ cm^{-1}$) and a negative band at 436 nm ($\Delta\varepsilon = -430\ M^{-1}\ cm^{-1}$) [Fig. 6(c)]. The intensity was further increased in solutions with a large porphyrin loading ($R < 10$). The presented dependence of the UV–visible, RLS and induced CD spectra on ionic strength and R indicates that **P_3** forms highly ordered extended assemblies on the DNA surface. Porphyrin–porphyrin interactions give rise to conservative signals, attributed to self-stacked porphyrin units oriented roughly perpendicular to the helix axis as originally proposed by Carvlin *et al.*[38] The DNA exterior acts as a template, which imposes structural packing of the porphyrin molecules to chiral assemblies. In addition, the UV–visible spectra indicate that **P_3** is bound also as a monomer; however, this form is not clearly resolved in the CD spectra because of strong overlapping features, making the resolution into the respective contributions impossible.

Surprisingly, at small R the contribution of aggregates was increased, as evidenced by decreasing absorbance of **P_3** monomer at 414 nm and increasing absorbance at 438 nm [Fig. 7(a)]. This effect was evident at low ionic strength and $R < 10$, where concentration of **P_3** is comparable to that of DNA base pairs. The DNA-induced assembling was also observed by adding DNA to a solution of exclusively monomeric **P_3**, i.e. at low ionic strength (cf. Fig. 8(a) and (b)] or at increased temperature (37 °C). These observations confirm the importance of cationic porphyrin–anionic matrix electrostatic interactions. The repulsion forces between positively charged substituents of **P_3** are compensated by attraction of the porphyrin units to the negatively charged DNA backbone. This effect is similar to that observed in solutions with high ionic strength where ions shield the positive charge of the pyridinium substituents resulting in the formation of aggregates.

Porphyrin **P_2** is more hydrophobic than **P_3**. As **P_2** was extensively aggregated in aqueous solutions, **P_2** formed predominantly extended assemblies on the DNA surface whereas the formation of bound monomer occurred very slowly.

The effects of deposited porphyrins on thermal denaturation of calf thymus DNA were studied by UV melting experiments (Fig. 8, inset). Whereas bound **P_3** was monomerized at temperatures near T_m [Fig. 8(c)], **P_2** remained predominantly self-assembled, as indicated by

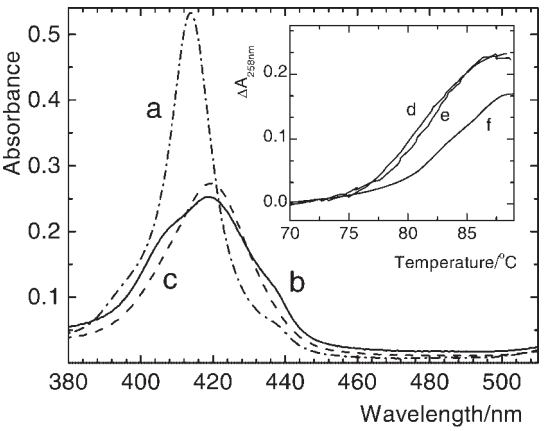

Figure 8. Absorption spectra of **P_3** (2 μM) in 20 mM phosphate buffer (pH 7.0), 50 mM NaCl, 25 °C (a), after addition of DNA (107 μM) at 25 °C (b) and after heating to 88 °C (c). Inset: Temperature dependent absorbance changes monitored at 258 nm: (d) 58 μM calf thymus DNA; (e) 58 μM calf thymus DNA, 2 μM **P_3**; (f) 56 μM calf thymus DNA, 3.4 μM TMPyP

spectral features of the porphyrin Soret bands. The spectra also indicated that both porphyrins were still bound to DNA [Fig. 8(c)]. We found that neither porphyrin influenced the melting profiles of DNA and the melting temperatures T_m. The T_m values in the presence ($R = 18–29$) and absence of porphyrins varied from 81 to 82 °C [Fig. 8(d) and (e)]. Under the same conditions, TMPyP, which intercalates between G–C base pairs, increased T_m to 83 °C [Fig. 8(f)]. The increase in T_m reflects stabilization of the double helix due to intercalation of the porphyrin moiety, which is in accordance with previous results.[1,37] Evidently, the outside binding and outside binding with self-stacking modes do not contribute to the thermal stability of double helical DNA.

In air-saturated aqueous solutions, the triplet states of **P₂**–**P₄** monomers were quenched by oxygen according to first-order kinetics (monoexponential) with a lifetime of ~2 μs (Table 1). In contrast, after binding to DNA, the triplet states decayed with biexponential kinetics characterized by two lifetimes. The lifetime of the faster process was coincident with oxygen quenching of free (unbound) porphyrin. The slower process was attributed to quenching of the triplet states of bound monomers (Table 1). The contribution of the respective processes varied according to the equilibrium molar ratio of free to DNA-bound monomer. The binding to DNA caused a marked increase in the triplet state lifetime, indicating the localization of the porphyrin molecules in a region with lower oxygen accessibility than in solution. The lifetimes of 17.1 μs (**P₃**) and 12.2 μs (**P₄**) in aerated solutions are comparable to those recorded for externally bound cationic porphyrins.[23,39,40] For comparison, the triplet state lifetimes of intercalated porphyrins are extended to 60 μs owing to the protection of excited porphyrin molecules by the nucleic acid duplex. Because bound **P₂** exists predominantly in the form of highly extended assemblies the formation of the triplet states was completely suppressed (see earlier).

As pointed out earlier, collisional quenching of the triplet states of porphyrin monomers by dissolved oxygen leads to $^1O_2$. The rise in the local concentration of $^1O_2$ is governed by the rate of triplet state quenching by oxygen. Because the triplet states of bound **P₃** and **P₄** are quenched more slowly than excited porphyrins in solution, the rates of formation and decay of $^1O_2$ became comparable, as follows from time-resolved luminescence experiments. Evidently, both **P₃** and **P₄** produced $^1O_2$ effectively also after external binding to DNA. This is in accordance with the fact that Φ_Δ is usually little affected by binding sensitizers to nucleic acids.[39,40]

CONCLUSION

Porphyrins **P₂** and **P₃** aggregate considerably in aqueous solutions whereas **P₄** remains monomeric and produces $^1O_2$ even at high ionic strength. Both H- and J-aggregates were resolved and characterized. The most hydrophilic porphyrin **P₄** is bound externally to the DNA backbone predominantly as a monomer. On the other hand, **P₂** and **P₃** form extended chiral assemblies on the DNA exterior. Nucleic acids with negatively charged phosphate groups shield repulsion forces between the porphyrin units that spontaneously assemble into helical assemblies deposited on the DNA surface. The helicity of the DNA backbone is imparted to the porphyrin assembly, resulting in induced chirality. Nucleic acids also facilitate the formation of J-aggregates when the concentrations of DNA in base pairs and porphyrin are comparable. The lifetimes of the triplet states of monomeric **P₃** and **P₄** increase after binding, however, this does not prevent the formation of $^1O_2$.

Acknowledgements

This research was supported by the Grant Agency of the Czech Republic (Grants 203/01/0634, 203/02/0420 and 203/04/0426). The authors thank Professor P. Anzenbacher, Jr, of the Center for Photochemical Studies, Bowling Green State University, for the synthesis of porphyrins, and Dr P. Maloň of the Institute of Organic Chemistry, ASCR, for the measurement of the CD spectra.

REFERENCES

1. Fiel RJ, Howard JC, Mark EH, Datta Gupta N. *Nucleic Acids Res*. 1979; **6**: 3093–3118.
2. Armitage B. *Chem. Rev*. 1998; **98**: 1171–1200.
3. Haq I, Trent JO, Chowdhry BZ, Jenkins TC. *J. Am. Chem. Soc*. 1999; **121**: 1768–1779.
4. Dass CR. *J. Pharm. Pharmacol*. 2002; **54**: 3–27.
5. Schweitzer C, Mehrdad Z, Noll A, Grabner E, Schmidt R. *J. Phys. Chem. A* 2003; **107**: 2192–2198.
6. Redmond RW, Gamlin JN. *Photochem. Photobiol*. 1999; **70**: 391–475.
7. Fiel RJ. *J. Biomol. Struct. Dyn*. 1989; **6**: 1259–1274.
8. Chen X, Liu M. *J. Inorg. Biochem*. 2003; **94**: 106–113.
9. Pasternack RF, Bustamante C, Collings PJ, Giannetto A, Gibs EJ. *J. Am. Chem. Soc*. 1993; **115**: 5393–5399.
10. Pasternack RF, Gibs EJ, Villafranca JJ. *Biochemistry* 1983; **22**: 2406–2414.
11. Maziere JC, Santus R, Morliere P, Reyftmann JP, Candide C, Mora L, Salmon S, Maziere C, Gatt S, Dubertret L. *J. Photochem. Photobiol. B* 1990; **6**: 61–68.
12. Králová J, Dvořák M, Král V. *J. Med. Chem*. 2003; **46**: 2049–2056.
13. Kasha M, Rawls HR, El-Bayoumi MA. *Pure. Appl. Chem*. 1965; **11**: 371–392.
14. Scholes GD. *Chem. Phys*. 2002; **275**: 373–386.
15. Ohno O, Kaizu Y, Kobayashi H. *J. Chem. Phys*. 1993; **99**: 4128–4139.
16. Akins DL, Zhu H, Guo Ch. *J. Phys. Chem*. 1996; **100**: 5420–5425.
17. Kano K, Minamizono H, Kitae T, Negi S. *J. Phys. Chem*. 1997; **101**: 6118–6124.
18. Kano K, Fukuda K, Wakami H, Nishiyabu R, Pasternack RF. *J. Am. Chem. Soc*. 2000; **122**: 7494–7502.
19. Kubát P, Lang K, Procházková K, Anzenbacher P Jr. *Langmuir* 2003; **19**: 422–428.

20. Tjahjono DH, Mima S, Akutsu T, Yoshioka N, Inoue H. *J. Inorg. Biochem*. 2001; **85**: 219–228.
21. Kubát P, Lang K, Anzenbacher P, Král V, Ehrenberg B. *J. Chem. Soc., Perkin Trans. 1* 2000; 933–941.
22. Kubát P, Lang K, Anzenbacher P. *J. Phys. Chem. B* 2002; **106**: 6784–6792.
23. Lang K, Anzenbacher P Jr, Kapusta P, Kubát P, Král V, Wagnerová DM. *J. Photochem. Photobiol. B* 2000; **57**: 51–59.
24. Wells RR, Larson JE, Grant RC, Shortle BE, Cantor CR. *J. Mol. Biol*. 1970; **54**: 465–497.
25. Gensch T, Viappiani C, Braslavsky SE. *J. Am. Chem. Soc*. 1999; **121**: 10573–10582.
26. Lemieux RU. *Acc. Chem. Res*. 1996; **29**: 373–380.
27. Kasha M. *Radiat. Res*. 1963; **20**: 55–70.
28. Ribó JM, Bofill JM, Crusats J, Rubires R. *Chem. Eur. J*. 2001; **7**: 2733–2737.
29. Schweitzer-Stenner R, Cupane A, Leone M, Lemke Ch, Schott J, Dreybrodt W. *J. Phys. Chem. B* 2000; **104**: 4754–4764.
30. Gregg BA, Fox MA, Bard AJ. *J. Am. Chem. Soc*. 1989; **111**: 3024–3029.
31. Knapp EW. *Chem. Phys*. 1984; **85**: 73–82.
32. Collings PJ, Gibbs EJ, Starr TE, Vafek O, Yee C, Pomerance LA, Pasternack RF. *J. Phys. Chem. B* 1999; **103**: 8474–8481.
33. Wilkinson F, Helman P, Ross AB. *J. Phys. Chem. Ref. Data* 1993; **22**: 113.
34. Ricchelli F. *J. Photochem. Photobiol. B* 1995; **29**: 109–118.
35. Nordén B, Kurucsev T. *J. Mol. Recognit*. 1994; **7**: 141–156.
36. Sehlstedt U, Kim SK, Carter P, Goodisman J, Vollano JF, Nordén B, Dabrowiak JC. *Biochemistry* 1994; **33**: 417–426.
37. Lugo-Ponce P, McMillin DR. *Coord. Chem. Rev.* 2000; **208**: 169–191.
38. Carvlin MJ, Datta-Gupta N, Fiel RJ. *Biochem. Biophys. Res. Commun*. 1982; **108**: 66–73.
39. Kruk NN, Dzhagarov BM, Galievsky VA, Chirvony VS, Turpin PY. *J. Photochem. Photobiol. B* 1998; **42**: 181–190.
40. Brun AM, Harriman A. *J. Am. Chem. Soc*. 1994; **116**: 10383–10393.